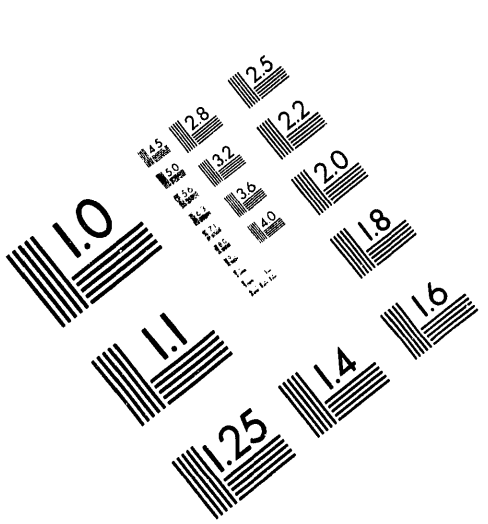

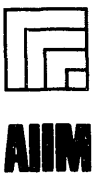

Association for Information and Image Management
1100 Wayne Avenue, Suite 1100
Silver Spring, Maryland 20910
301/587-8202

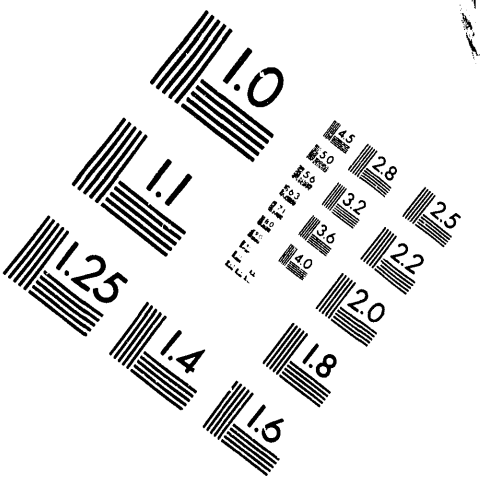

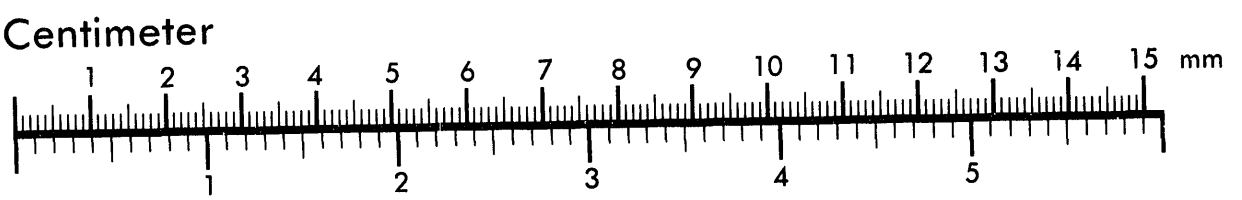

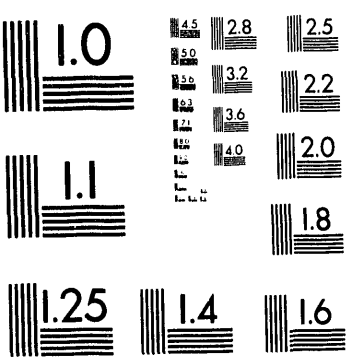

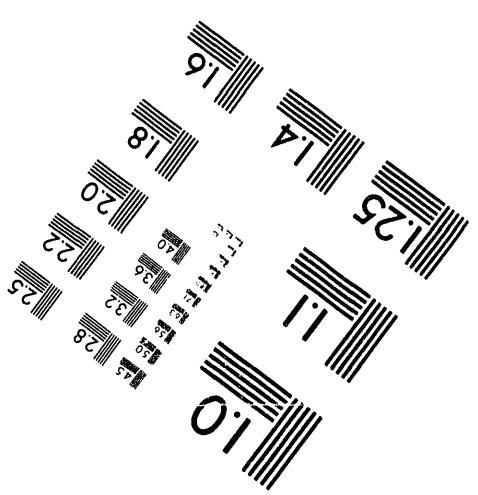

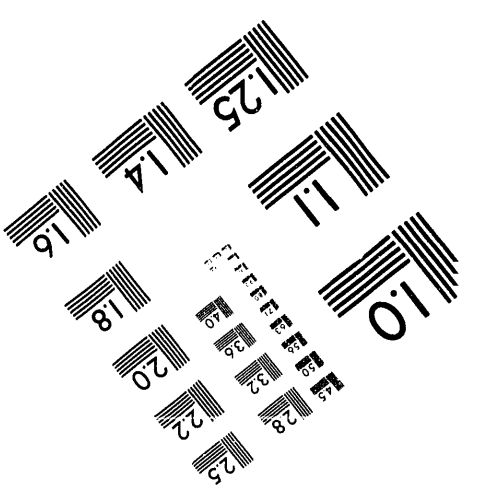

1 of 1

2.

Conf-930702--44

DRAFT
Paper to be presented at
ASME Pressure Vessel & Piping
Meeting, Denver, CO., July 26-30, 1993

ASSESSMENT OF AN IMPROVED MULTIAXIAL STRENGTH THEORY BASED ON CREEP-RUPTURE DATA FOR INCONEL 600[1]

R. L. Huddleston

Engineering Technology Division
Oak Ridge National Laboratory
Oak Ridge, Tennessee

ABSTRACT

A new multiaxial strength theory incorporating three independent stress parameters was developed and reported by the author in 1984. It was formally incorporated into ASME Code Case N47-29 in 1990. The new theory provided significantly more accurate stress-rupture life predictions than obtained using the classical theories of von Mises, Tresca, and Rankine (maximum principal stress), for Types 304 and 316 stainless steel tested at 593 and 600°C respectively under different biaxial stress states. Additional results for Inconel 600 specimens tested at 816°C under tension-tension and tension-compression stress states are presented in this paper and show a factor of approximately 2.4 reduction in the scatter of predicted versus observed lives as compared to the classical theories of von Mises and Tresca and a factor of about 5 as compared to the Rankine theory. A key feature of the theory, which incorporates the maximum deviatoric stress, the first invariant of the stress tensor, and the second invariant of the deviatoric stress tensor, is its ability to distinguish between life under tensile versus compressive stress states.

INTRODUCTION

A new multiaxial strength theory was developed by the author and initially reported in 1984 [1] with an additional assessment reported in 1992 [2]. The theory incorporates four stress parameters which can be formulated from the three independent stress parameters: maximum deviatoric stress (S_1), the first stress invariant (J_1), and the second deviatoric stress invariant (J_2'). The theory distinguishes between tensile ($J_1>0$) and compressive ($J_1<0$) stress states which is not possible using the classical strength theories of Tresca (maximum shear stress) and von Mises (octahedral shear stress) [3]. The new theory was previously shown by the author to provide significantly improved creep-rupture life predictions in tests of Type 304 [1] and 316 [2] stainless steel conducted under constant-load conditions at 593 and 600°C respectively. During 1990 the theory was incorporated into ASME Code Case N47 [4] for use in computing creep-rupture damage and life in elevated temperature components. In the current paper the accuracies of both the new and classical theories are assessed for predicting creep-rupture life in biaxial tests of annealed Inconel 600 conducted under constant-load conditions at 816°C in argon.

Prior investigations of multiaxial creep-rupture behavior include the works of Chubb and Bolton [5], Kennedy, Harms, and Douglas [6], Sdobyrev as referenced by Rabotnov [7], Davis [8], Johnson, Henderson, and Khan [9], Rowe, Stewart, and Burgess [10], Abo El Ata and Finnie [11], Hayhurst [12], Anderson, Atkins, and Shavely [13], Hayhurst, Leckie, and Morrison [14], and others. Manjoine [15] has similarly investigated the stress-state problem and has provided a summary with discussions of selected strength theories which have been proposed over the years. Rowe, et al. and Anderson, et al. investigated creep rupture in tubes of Types 304 and 316 stainless steel under biaxial tension-tension stress states. The classical theories of von Mises, Tresca, and Rankine differ by less than ~ 15 percent for these stress states. Chubb, et al. and Kennedy, et al. investigated creep rupture in tubes of Type 316 stainless steel and Inconel respectively, under both biaxial tension-tension and compression-tension stress states thus covering an area of stress space where greater differences exist

[1]Work performed by Oak Ridge National Laboratory for the U.S. Department of Energy under contract DE-AC05-84OR21400 with Martin Marietta Energy Systems.

between the Rankine theory as compared to the Tresca and von Mises theories. Choice of a best strength theory in these and most of the previously referenced investigations tended to be both material and temperature dependent with all three of the previously noted classical theories selected as being the best candidate for at least one test material and one test temperature. The classical theories all provide a relatively poor fit to the data for compression-tension stress states.

Several key investigations which have provided a base of mechanistic support for the current work are those of Cane [16], Speight and Beere [17], Beere and Speight [18], Hellan [19], and Dyson [20]. In particular Cane's publication was very useful. Cane, in referencing the other cited authors' work, summarizes the stages of fracture by the classical grain boundary cavitation process as being the production of cavity nuclei (Stage I), the deformation of stable cavities and their growth to produce discrete cracks (Stage II), and linkage of discrete cracks to produce final fracture (Stage III). In terms of continuum mechanics variables, Cane relates the stress state dependence of these processes to the von Mises equivalent stress, $\bar{\sigma}$, the hydrostatic stress, $J_1/3$, the maximum principal stress, σ_1, and the maximum deviatoric stress, S_1. In development of the author's strength theory, these same stress parameters, when appropriately formulated, have resulted in significantly improved life predictions relative to the three previously noted classical theories.

The balance of this paper summarizes the improved strength theory, the experimental Inconel 600 creep-rupture data on which the current theory assessments are based, assessment results, and some brief conclusions.

STRENGTH THEORY

For a multiaxial stress state with ordered principal stresses $\sigma_1 > \sigma_2 > \sigma_3$, the new strength theory defines the uniaxially equivalent stress as

$$\sigma_e = \frac{3}{2} S_1 \left(\frac{2}{3}\frac{\bar{\sigma}}{S_1}\right)^a \exp\left[b\left(\frac{J_1}{S_1} - 1\right)\right] \qquad (1)$$

where

$$J_1 = \sigma_1 + \sigma_2 + \sigma_3 \qquad (2)$$

$$= 3\sigma_{oct}$$

$$\bar{\sigma} = \sqrt{[(\sigma_1-\sigma_2)^2 + (\sigma_2-\sigma_3)^2 + (\sigma_3-\sigma_1)^2]/2} \qquad (4)$$

$$= \sqrt{3J'_2}$$

$$S_1 = \sigma_1 - \frac{J_1}{3} \qquad (4)$$

$$= \sigma_1 - \sigma_{oct}$$

and

$$S_s = \sqrt{\sigma_1^2 + \sigma_2^2 + \sigma_3^2} \qquad (5)$$

$$= \sqrt{(6J'_2 + J_1^2)/3}$$

$$= \sqrt{J_1^2 - 2J_2}$$

$$= \sqrt{3J_2' + J_2}$$

$$= \sqrt{3(\sigma_{oct}^2 + \tau_{oct}^2)}$$

and

J_1 = 1st invariant of the stress tensor,
J_2 = 2nd invariant of the stress tensor,
J_2' = 2nd invariant of the deviatoric stress tensor,
S_1 = maximum deviatoric stress,
$\bar{\sigma}$ = von Mises equivalent stress,
σ_{oct} = normal stress on octahedral plane, and
τ_{oct} = shear stress on octahedral plane.

For a = 1.0, the new theory reduces to the form

$$\sigma = \bar{\sigma} \exp[b(J_1/S_s - 1)] \qquad (6)$$

which removes any dependence of σ_e on maximum deviatoric stress, S_1, while maintaining dependence on the hydrostatic stress component, J_1 (or octahedral normal stress), and the octahedral shear stress, J_2' (or $\bar{\sigma}$). Parameters $\bar{\sigma}$, J_1, and S_s are all stress invariants (i.e., can be expressed in terms of the principal invariants of the stress tensor).

The invariant stress parameters in the new theory (J_1, S_s, and $\bar{\sigma}$) are graphically illustrated in Fig. 1. Parameters a and b are constants which can vary slightly from material to material. For best life predictions, the constants can be determined by a least-squares fit of the theory to multiaxial stress-rupture data for a range of stress states. A minimum of two test points are required to fit the constants a and b in Eq. 1, with the recommended tests being one torsion and one equal biaxial tension test, or a minimum of one test is required to fit the constant b in Eq. 6 with the recommended test being a pure torsion test. Stress parameters incorporated in the new theory have been shown by Cane and others to correlate with the mechanistic creep-rupture processes of cavity formation, growth, linkage, and failure [1, 16-20].

Five materials (two ferritic steels and three nickel-base alloys) have been studied to date and have been found to have somewhat universal values of a and b for creep-rupture life predictions. Results for Types 304 and 316 stainless steel, Inconel 600, modified 9 Cr-1 Mo steel, and 2 1/4 Cr-1 Mo steel have indicated that parameter a tends to have a value in the range of 0.85-1.10 with 1.0 being a good universal value to use in the absence of data to define a "best fit" value. A value of a = 1.0 also assures one that the shape of the "prismatic" 3-D isochronous failure surface in σ_1, σ_2, σ_3 space will be circular in planes of constant J_1 similar to contours for the von Mises strength theory. Parameter b tends to have a value in the 0.15-0.30 range for the previously noted materials. The value of b determines the appropriate magnitude of the hydrostatic-stress effect in the strength theory, thus determines differences in equivalent stress and life under tensile ($J_1>0$) versus compressive ($J_1<0$) stress states. The author has found that life predictions made using the new strength theory are significantly better than predictions made using the previously noted classical theories both when the optimum constants a and b are used and also when the universal values of $a=1.00$ and $b=0.24$ are used.

In general, time to creep-rupture, t_r, is approximately linear in log (time) versus log (stress) space and was, therefore, represented for the purposes of this paper by the equation

$$\log(t_r) = A_0 + A_1 \log(\sigma_e) \qquad (7)$$

where σ_e denotes the "uniaxially equivalent" stress. Consistent

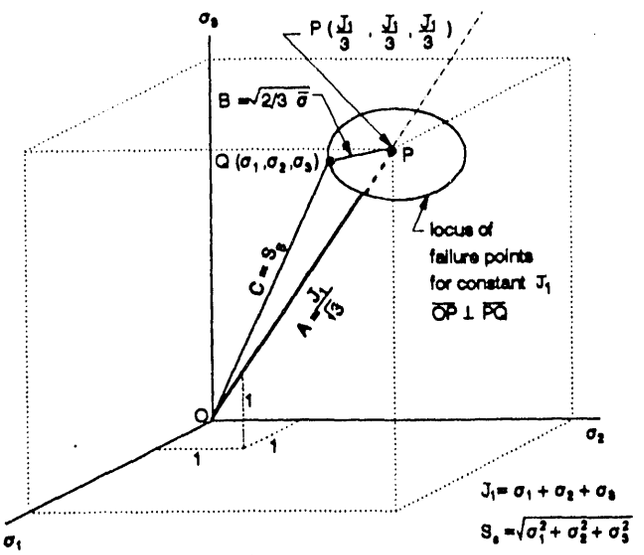

FIG. 1 GEOMETRIC REPRESENTATION OF NEW STRENGTH MODEL STRESS PARAMETERS

with the usual design approach, constants A_0 and A_1 are defined by a least-squares fit of Eq. 7 to baseline uniaxial creep-rupture data. It is then assumed that a complex multiaxial stress state can be reduced mathematically, through the "strength theory" (Eq. 1 or Eq. 6) to a uniaxially equivalent value σ_e such that the uniaxial correlation (Eq. 7) in conjunction with the equivalent stress from Eq. 1 (or Eq. 6) can be used to predict the failure time for a component under a complex multiaxial stress state. For the assessments presented in this paper, it is assumed that the time required to initiate a crack is approximately equal to the rupture time for the biaxial tubular test specimens.

MATERIAL AND SPECIMEN

Assessments of the strength theories reported in this paper are based on test results for annealed Inconel 600 as reported by Kennedy, Harms, and Douglas [6]. The nominal composition of the Inconel 600 material utilized in their tests was 80 Ni-15 Cr-5 Fe. Their tubular specimens were nominally 21.4-mm inside diameter, 1.52-mm wall thickness, and 63.5-mm gage length.

EXPERIMENTAL DATA

Tests reported by Kennedy et al. were conducted in argon at 816°C under constant-load conditions. Uniaxial tests were conducted using the same tubular specimen design as used for their biaxial tests. Four tests were conducted under a pure axial load to produce uniaxial tension in the tube. Three tests were conducted under a combination of axial compression and internal pressure which produced a "pure" hoop stress with zero axial stress. These seven tests provided the data for development of a baseline "uniaxial" stress rupture correlation

(i.e. the small radial stress in the "pure" hoop stress tests was ignored). The biaxial tests of Kennedy et al. were performed under combinations of axial load (tension and compression) and internal pressure. Their stress rupture results, from some 45 tests, are summarized in Table 1. Since the seven "uniaxial" tests were conducted using a tubular specimen rather than a conventional uniaxial solid bar specimen, these seven data points were included in the biaxial data set used for strength theory assessments.

To use the individual biaxial test data in Table 1 to objectively assess stress state effects, the effects of material and testing variability should be minimized. As was done in the author's prior publications [1,2], an "averaged biaxial data set" was created from the data in Table 1. This was accomplished by linearly averaging, in log (stress) versus log (rupture time) space, each subset of the biaxial test data having the same stress state (i.e., the same biaxial stress ratio, $R=\sigma_\theta/\sigma_z$). This reduced the 45 data in Table 1 to the 20 data points summarized in Table 2 with only one representative point for each independent stress state.

A least-squares fit of the linear stress-rupture equation (Eq. 7) to the seven uniaxial data in Table 1 resulted in the baseline uniaxial stress-rupture correlation given by:

$$\log(t_r)=9.1830-4.3034\ \log(\sigma) \qquad (8)$$

Since the "pure" hoop stress rupture data tended to form a stress rupture line falling below (i.e., shorter lives) the axial tension data, a lot-centered fitting technique was used to determine the slope of the uniaxial line in Eq. 8. Using this technique, the average value of $\log(t_r)$ and $\log(\sigma)$ for each subset (i.e. each lot of data) was subtracted from the individual data values for the lot. A least-squares fit of the resulting combined data sets determined the "lot-centered slope" representing all the fitted data. The intercept constant, 9.1830, was then determined by forcing the stress rupture line with the lot-centered slope to pass through the centroid of the total uniaxial data set (i.e., through the average $\log(t_r)$ and average $\log(\sigma)$ point for the total uniaxial data set). The resulting data correlation is given in Eq. 8 and is plotted in Fig. 2.

RESULTS

As in the author's two prior publications [1,2], results of the assessment of the new versus the classical strength theories are summarized in four comparative forms: (1) standard 2-D biaxial isochronous stress-rupture contours; (2) polar plots of deviations in the ratio of predicted-to-observed life as a function of stress state showing which stress states result in the best and worst life predictions; (3) the usual logarithmic stress versus rupture time correlations; and (4) a statistical assessment of the new and classical theories partitioning the total error between predicted and observed life into a strength theory error, which is dependent on stress state, and a random error, which is attributed to material and testing variability.

TABLE 1 SUMMARY OF BIAXIAL STRESS-RUPTURE DATA FOR ANNEALED INCONEL 600 TESTED AT 816°C

Test No.	$R=\frac{\sigma_\theta}{\sigma_z}$	σ_z (MPa)	σ_θ (MPa)	σ_r (MPa)	t_r (h)	Specimen Loading Mode **
1	0.00	41.370	0.000	0.000	169.0	AT
2	0.00	41.370	0.000	0.000	330.2	AT
3	0.00	27.580	0.000	0.000	2140.0	AT
4	0.00	20.685	0.000	0.000	4490.6	AT
5	0.17	41.370	6.895	-0.490	249.0	AT & P
6	0.25	27.580	6.895	-0.490	1840.0	AT & P
7	0.50	41.370	20.685	-1.476	231.0	AT & P
8	0.50	34.475	17.238	-1.227	635.0	AT & P
9	0.50	27.580	13.790	-0.979	982.0	AT & P
10	0.50	27.580	13.790	-0.979	1640.0	AT & P
11	0.50	20.685	10.343	-0.738	3900.0	AT & P
12	0.67	41.370	27.580	-1.965	317.0	AT & P
13	0.75	27.580	20.685	-1.476	717.0	AT & P
14	1.00	41.370	41.370	-2.944	91.2	AT & P
15	1.00	27.580	27.580	-1.965	649.0	AT & P
16	1.00	20.685	20.685	-1.476	2785.8	AT & P
17	1.00	20.685	20.685	-1.476	3124.0	AT & P
18	1.20	34.475	41.370	-2.944	134.0	AT & P
19	1.33	20.685	27.580	-1.965	601.3	AT & P
20	1.50	27.580	41.370	-2.944	128.0	AT & P
21	1.60	17.238	27.580	-1.965	666.0	AT & P
22	1.71	24.133	41.370	-2.944	125.3	AT & P
23	1.85	22.409	41.370	-2.944	106.2	AT & P
24	2.00	20.685	41.370	-2.944	79.0	AT & P
25	2.00	20.685	41.370	-2.944	85.0	AT & P
26	2.00	13.790	27.580	-1.965	629.0	AT & P
27	2.00	10.343	20.685	-1.476	1672.0	AT & P
28	4.00	10.343	41.370	-2.944	160.0	AT & P
29	4.00	10.343	41.370	-2.944	190.7	AT & P
30	4.00	6.895	27.580	-1.965	398.6	AT & P
31	4.00	6.895	27.580	-1.965	487.0	AT & P
32	4.00	5.171	20.685	-1.476	1811.9	AT & P
33	∞	0.000	41.370	-2.944	98.0	AT & P
34	∞	0.000	27.580	-1.965	546.0	AT & P
35	∞	0.000	20.685	-1.476	1696.0	AT & P
36	-0.25	-55.160	13.790	-0.979	168.9	AC & P
37	-1.00	-41.370	41.370	-2.944	47.6	AC & P
38	-1.00	-27.580	27.580	-1.965	235.0	AC & P
39	-1.00	-20.685	20.685	-1.476	1290.0	AC & P
40	-2.00	-20.685	41.370	-2.944	69.2	AC & P
41	-2.00	-20.685	41.370	-2.944	154.0	AC & P
42	-2.00	-13.790	27.580	-1.965	308.0	AC & P
43	-2.00	-10.343	20.685	-1.476	1221.0	AC & P
44	-4.00	-6.895	27.580	-1.965	479.3	AC & P
45	-4.00	-6.895	27.580	-1.965	668.4	AC & P

* Source: Kennedy, Harms, and Douglass, Ref. 6

** AT = axial tension

AC = axial compression

P = internal pressure

TABLE 2 AVERAGED BIAXIAL STRESS-RUPTURE DATA FOR ANNEALED INCONEL 600 TESTED AT 816° C

Data Subset No.	$R=\frac{\sigma_\theta}{\sigma_z}$	σ_z (MPa)	σ_θ (MPa)	σ_r (MPa)	t_r (h)	Specimen Loading Mode **
1	0.00	31.434	0.000	0.000	855.7	AT
2	0.17	41.370	6.895	-0.490	249.0	AT & P
3	0.25	27.580	6.895	-0.490	1840.0	AT & P
4	0.50	29.529	14.764	-1.048	983.7	AT & P
5	0.67	41.370	27.580	-1.965	317.0	AT & P
6	0.75	27.580	20.685	-1.476	717.0	AT & P
7	1.00	26.432	26.432	-1.885	847.2	AT & P
8	1.20	34.475	41.370	-2.944	134.0	AT & P
9	1.33	20.685	27.580	-1.965	601.3	AT & P
10	1.50	27.580	41.370	-2.944	128.0	AT & P
11	1.60	17.238	27.580	-1.965	666.0	AT & P
12	1.71	24.133	41.370	-2.944	125.3	AT & P
13	1.85	22.409	41.370	-2.944	106.2	AT & P
14	2.00	15.716	31.431	-2.242	289.9	AT & P
15	4.00	7.655	30.620	-2.184	403.8	AT & P
16	∞	0.000	28.683	-2.046	449.4	AT & P
17	-0.25	-55.160	13.790	-0.979	168.9	AC & P
18	-1.00	-28.684	28.684	-2.046	243.5	AC & P
19	-2.00	-15.717	31.434	-2.240	251.6	AC & P
20	-4.00	- 6.895	27.580	-1.965	566.0	AC & P

* Source: Kennedy, Harms, and Douglas, Ref. 6

** AT = axial tension
AC = axial compression
P = internal pressure

A nonlinear least-squares fit (based on Eq. 7) of the new theory (Eq. 1) to the averaged Inconel data set in Table 2 resulted in "optimum" values $a=0.9984$ and $b=0.2481$. These constants were used for assessments 1-4 noted above. For assessment 4 two other sets of constants were also evaluated The second set of constants consisted of the assigned value of $a=1.00$ and the value of $b=0.2480$ obtained from a nonlinear least-squares fit of Eq. 7 to the averaged biaxial data set in Table 2. The third set consisted of the assigned values of $a=1.00$ and $b=0.24$, which the author has used as universal constants in the two prior papers [1,2], since they were not fitted to the material data sets. The accuracy of the new theory is not highly sensitive to small changes in these values. Constants of $a=1.0859$ and $b=0.2893$ were previously determined for annealed Type 304 stainless steel [1] and values of $a=0.8631$ and $b=0.2058$ previously determined for annealed Type 316 stainless steel [2]. The universal values of $a=1.0$ and $b=0.24$, although not optimum values, still result in significantly better life predictions for Types 304 and 316 stainless steel and Inconel 600 than the classical theories; However, life predictions were not quite as accurate as obtained using the alloy-specific

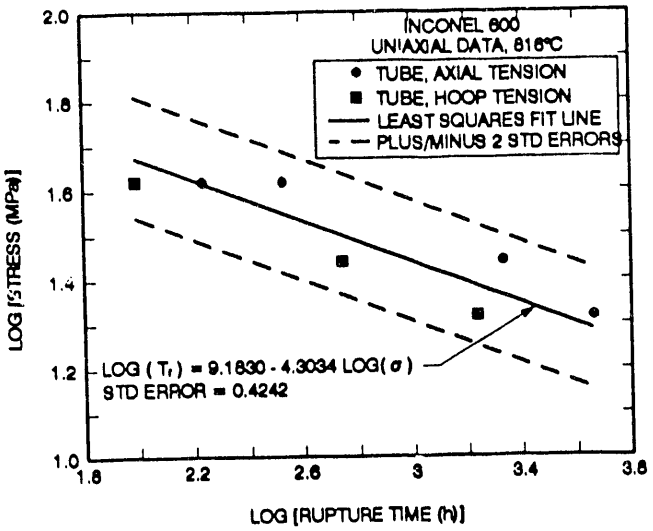

FIG 2 BASELINE UNIAXIAL STRESS VERSUS RUPTURE TIME DATA

values. Since the values of constants a and b for Inconel were almost identical for the three cases where (1) optimum values of both a and b were obtained from a least-squares fit, (2) the value of $a=1.00$ was assigned and b obtained from a least-squares fit, and (3) universal values of $a=1.00$ and $b=0.24$ were assigned (no fit), only the optimum values of $a=0.9984$ and $b=0.2481$ were used for the assessments summarized in this paper.

Isochronous Stress-Rupture Contour

Biaxial isochronous stress-rupture contours for both the new and the classical strength theories are shown in Fig. 3. Each averaged data point from Table 2 was shifted along a stress rupture line of slope $A_1=-4.3034$ (i.e., slope of the uniaxial stress rupture line, from Eq. 8) to a common rupture time, and the resulting isochronous biaxial stress point plotted in Fig. 3. One can see that the new theory fits the Inconel data significantly better than the classical theories in the second and fourth quadrants for the tension-compression stress states. This was also true for the 304 and 316 stainless steel results reported previously. In the first quadrant, neither the classical strength theories or the new theory represent the data very accurately. The data trend in the first quadrant for biaxial stress ratios in the range $2 \le \sigma_\theta/\sigma_z \le \infty$ does not follow the usual data trend [1,2]. It is possible that instability may have influenced the data, however no attempt was made by the author to investigate the instability problem. Internal pressure also results in tube diameter growth during a test which continuously alters the biaxial stress ratio during the test. This was not taken into account in the correlations developed in this paper. The data trend in quadrant 1 of Fig. 3, if real, would indicate significant anisotropy in Inconel 600 since the contour is not symmetrical about a 45° line. The agreement demonstrated by Types 304 and 316 stainless steel in quadrants 1, 2, and 4, as reported in

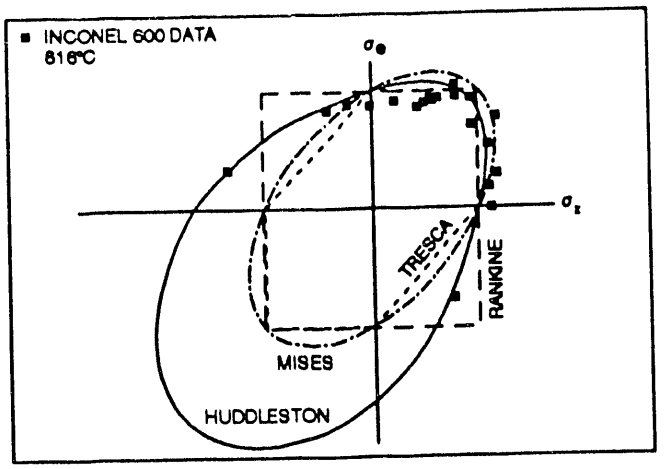

FIG. 3 BIAXIAL ISOCHRONOUS STRESS-RUPTURE CONTOUR FOR INCONEL 600

the author's two previous publications [1,2], was significantly better than is demonstrated in Fig. 3 for the Inconel data.

The 3-D isochronous rupture surface for Inconel 600 has a geometric "bottle shape" similar to that reported previously for Type 304 stainless steel and reproduced in Fig. 4 [1]. The bottle shape indicates larger stresses under compressive stress states than under tensile stress states for the same rupture time.

Polar Plots

Polar plots provide an excellent means for displaying deviations between predicted and observed life as a function of the biaxial stress state. Plots of this type, based upon the averaged data set in Table 2, are given in Figs. 5-8 for the new and classical strength theories. The ratio of predicted-to-observed rupture time is plotted radially in logarithmic scale with the plot axes and angle mapping the principal stress axes in the tubular specimen wall. For each biaxial test, the tangent of angle, Θ, in the polar plot is equal to the biaxial stress ratio in the specific test. For a perfect strength theory the data would fall on a circle of radius 10^0 (i.e., predicted life equals observed life). A circle (labeled as SM-20), denoting a safety margin of 20 on life (approximate safety margin in Appendix T of ASME Code Case N-47 [3]), is placed on each plot for reference. Similarly, a circle (labeled OCM-5) is shown on each plot and denotes an arbitrarily selected margin of 5 on life as a reference for overly conservative design.

A comparison of the four polar plots shows that the new theory (Fig. 5) did an excellent overall job of modeling stress-state effects in Inconel 600 both in terms of a lack of excessive conservatism and minimum erosion of a safety margin of 20 on life (i.e., the points all fall close to the 10^0 circle). In comparison, both the Tresca and the von Mises theories (Figs. 6 and 7 respectively) gave highly conservative life predictions for biaxial tension-compression (T-C) stress states (i.e., in second quadrant) and were also slightly less accurate than the new theory for tension-tension (T-T) stress states (i.e., in first

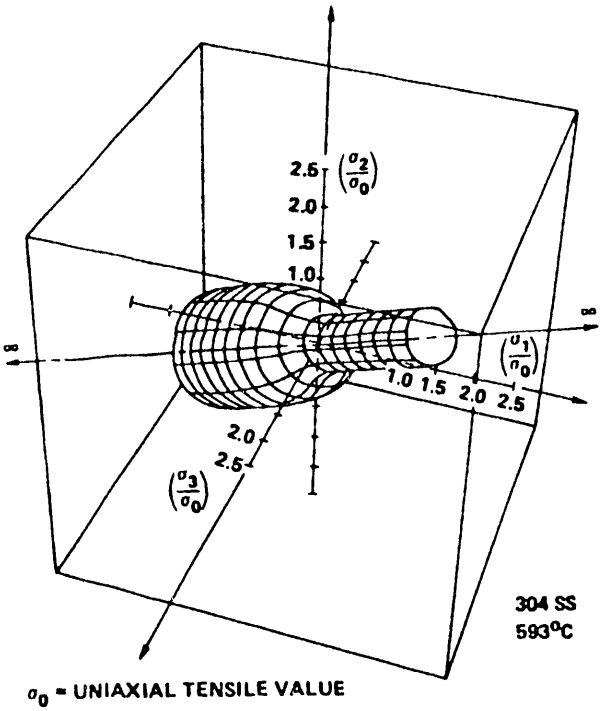

FIG. 4 THREE-DIMENSIONAL ISOCHRONOUS STRESS-RUPTURE SURFACE FOR TYPE 304 STAINLESS STEEL

quadrant). The Rankine theory provided significant life overpredictions under some T-C stress states while providing a significant life under prediction for at least one T-C stress state. The trends demonstrated in the first quadrant (for T-T stress states) were somewhat similar for all the strength theories with the new theory being slightly better at reducing the data scatter. Overall, these general trends which were observed in Inconel are very similar to the trends previously observed and reported by the author for Type 304 and 316 stainless steel.

Stress-Rupture Plots

Stress versus rupture time correlations for the new and the three classical strength theories are given in Figs. 9-12. These plots compare predicted specimen lives to observed lives for all the biaxial data summarized in Table 1. Since these correlations are based on individual test results rather than on the averaged data set (Table 2), they encompass the total scatter due to inaccuracy of the strength theory in precisely predicting stress-state effects as well as the scatter introduced by material and testing variability. The baseline uniaxial stress-rupture correlation (Eq. 8) is shown on each plot as a solid line and represents the predicted life line. The individual data are plotted in each figure. Each plot contains one dashed and two dotted lines. The dashed line is a least-squares fit of the biaxial data in Table 1, based on the specific strength theory noted in

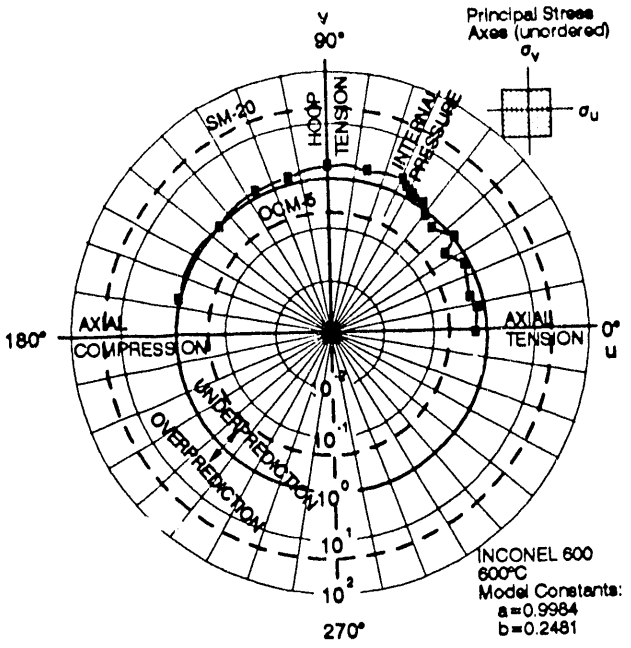

FIG. 5 CORRELATION OF THE RATIO OF PREDICTED TO OBSERVED LIFE WITH STRESS STATE BASED ON THE NEW THEORY

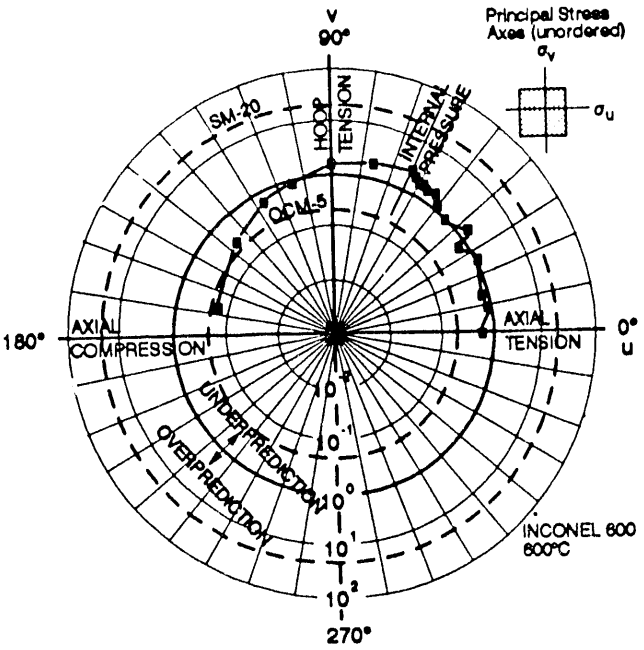

FIG. 7 CORRELATION OF THE RATIO OF PREDICTED TO OBSERVED LIFE WITH STRESS STATE BASED ON THE VON MISES THEORY

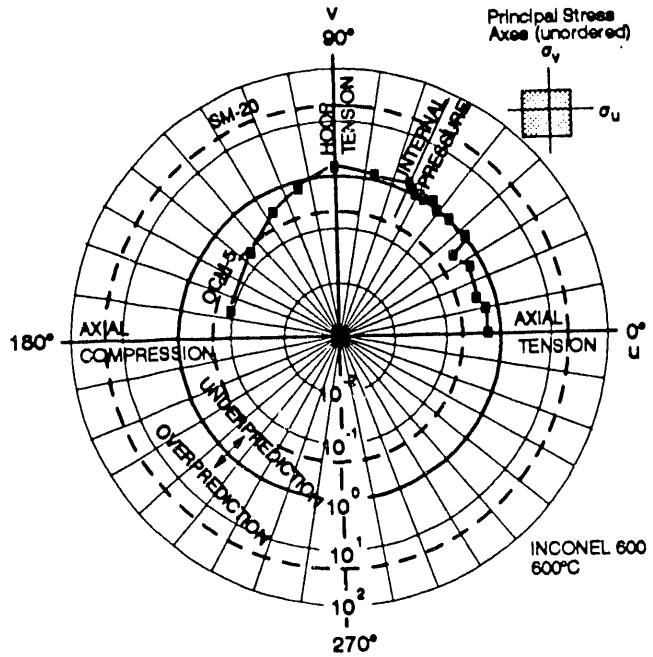

FIG. 6 CORRELATION OF THE RATIO OF PREDICTED TO OBSERVED LIFE WITH STRESS STATE BASED ON THE TRESCA THEORY

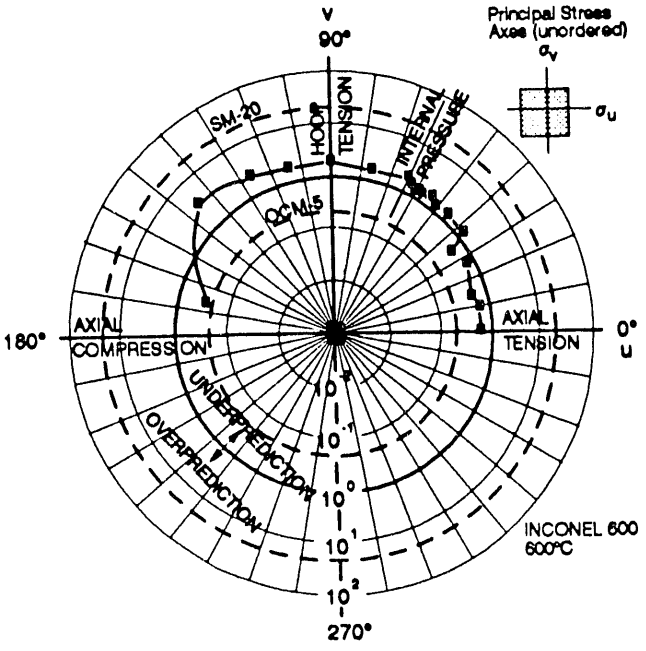

FIG. 8 CORRELATION OF THE RATIO OF PREDICTED TO OBSERVED LIFE WITH STRESS STATE BASED ON THE RANKINE THEORY

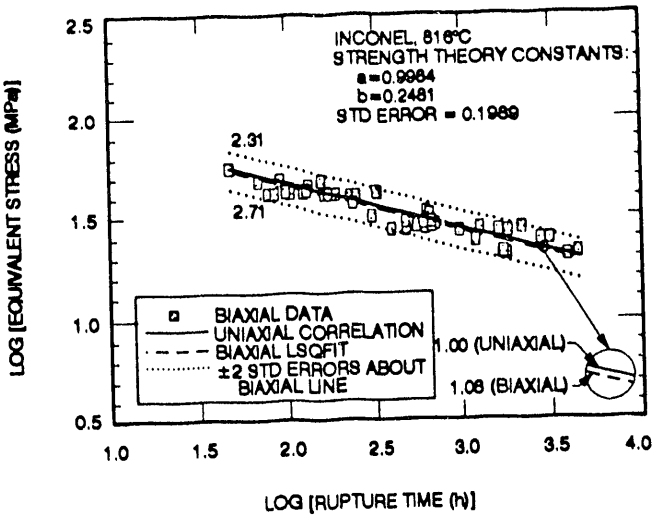

FIG. 9 EQUIVALENT STRESS VERSUS BIAXIAL RUPTURE TIMES FOR THE NEW STRENGTH THEORY

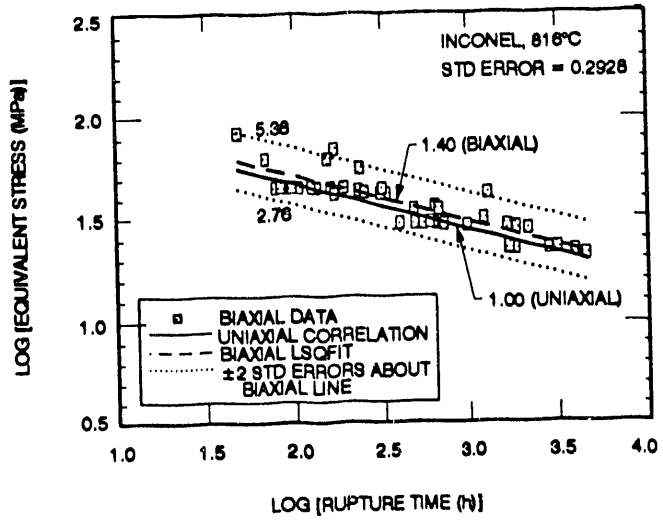

FIG. 10 TRESCA STRESS INTENSITY VERSUS BIAXIAL RUPTURE TIMES

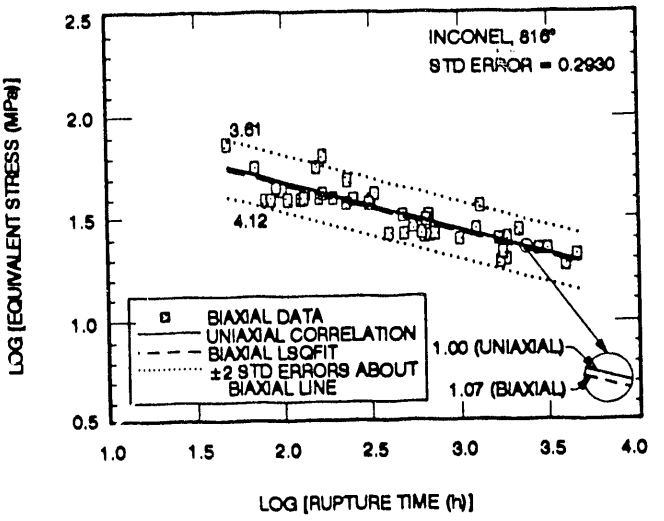

FIG. 11 VON MISES EQUIVALENT STRESS VERSUS BIAXIAL RUPTURE TIMES

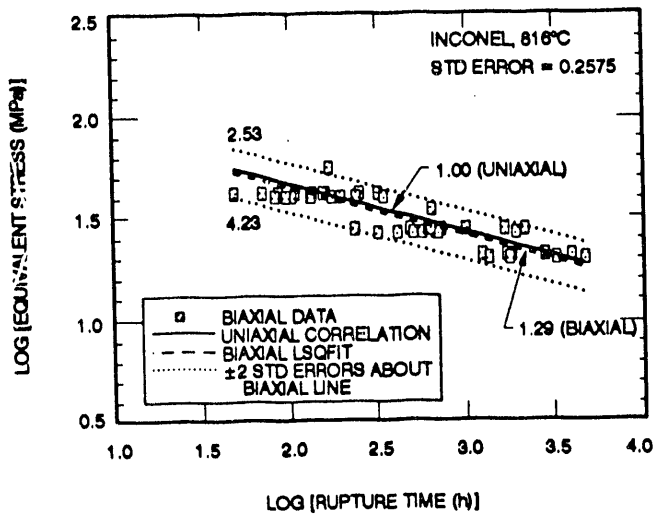

FIG. 12 MAXIMUM PRINCIPAL STRESS VERSUS BIAXIAL RUPTURE TIMES

the plot, assuming the biaxial line has the same slope A_1 as the uniaxial (solid) baseline. The two dotted lines represent ±2 statistical standard errors (denoted as ±2 S_y) relative to the dashed (biaxial) line. The dashed and dotted lines thus represent, respectively, the observed mean biaxial behavior and the scatter bounds within which about 95% of the biaxial data should fall. The scatter bounds, although symmetric relative to the biaxial (dashed) line are asymmetric relative to the predicted (uniaxial, solid) line. Each of the scatter bounds can thus be represented as a factor on life relative to the predicted life line (i.e., a factor above or below the predicted life). These factors are noted on each plot to facilitate a comparison of the strength theories. The total "range of scatter" is obtained by dividing the upper bound life by the lower bound life (i.e., by multiplying the two factors on the dotted lines given in each plot).

For these analyses the S_y for each strength theory was computed using the standard statistical equation

$$S_y = \sqrt{\frac{SSQDev}{\nu}} \qquad (9)$$

where

$$SSQDev = \sum_{i=1}^{N} (Dev)_i^2 \qquad (10)$$

$$Dev_i = [\log(t_R)_{pred} - \log(t_R)_{obs}]_i \qquad (11)$$

and degrees of freedom, ν, is given by

$$\nu = N - k \qquad (12)$$

N is the total number of data, and k is the number of material parameters (constants) obtained from the least-squares fit. Since the slope of the biaxial line is assumed to be the same as the uniaxial line, only the biaxial line intercept constant was fitted along with the constants in the strength theory. For the classical theories no constants were fitted, thus only the biaxial line intercept constant was fitted to the data, giving $\nu = N-1$. For the new theory, if both parameters a and b were fitted along with the biaxial line intercept, then $\nu = N-3$, whereas if parameter a was fixed as 1.0 and only b fitted, then $\nu = N-2$.

From the stress versus rupture time correlations given in Figs. 9-12, it is apparent that the new strength theory is more accurate than the three classical theories in predicting life and, therefore, in reducing data scatter. The data scatter range for the new theory is 6.26 as compared to ranges for the classical theories of 14.85 (Tresca), 15.20 (von Mises), and 30.83 (Rankine). For these data, the new theory, thus, reduced the scatter by a factor of about 2.4 on life relative to the von Mises and Tresca theories, which are the two most widely used strength theories used in high-temperature structural design codes.

Partitioning of Error

It is of interest to partition the total error between predicted and observed life into two components, one due to error in the strength theory and the second due to random scatter which is attributed to material and testing variability. A statistical model [linear in log (stress) vs log (rupture time) space] was used for this purpose. The model will be briefly described after which the results will be presented.

The total biaxial data set (Table 1) consisting of N data points is partitioned into m subsets with the data in each subset having the same stress state. Each subset, j, has n_j data points. The centroid (average log) of the n_j data in subset j is denoted as $(\bar{X}_j, \bar{Y}_j)$. It is assumed that the biaxial data in each subset falls along a unique stress-rupture line having the same slope, A_1, as the uniaxial data correlation, Eq. 8. Given these assumptions, which can be shown to be valid for the present

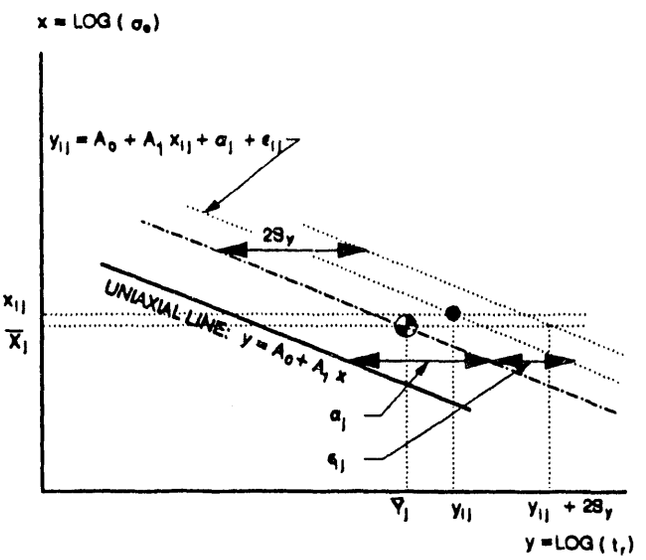

FIG. 13 STATISTICAL MODEL PARAMETERS

data, the model can be expressed by the following equation and is depicted graphically in Fig. 13:

$$y_{ij} = A_0 + A_1 x_{ij} + \alpha_j + \epsilon_{ij} \qquad (13)$$

The first two terms $(A_0 + A_1 x_{ij})$ in Eq. 13 are the uniaxially predicted part of y_{ij}. Parameter α_j represents the error due to inaccuracy of the strength theory for subset j. The last term represents the random error which is ascribed to material and testing variability. The standard error, S_y, determined from the random error values, ϵ_{ij}, was calculated in the usual manner according to the equation

$$S_y = \sqrt{\frac{\sum_{j=1}^{m}\sum_{i=1}^{n_j} \epsilon_{ij}^2}{N-k}} \qquad (14)$$

where $N-k$ denotes the number of degrees of freedom. To be statistically correct, two or more data points are needed at each stress state in order to estimate the average behavior and partition the total error into theory and random components. There are only nine data subsets of this type in Table 1. These nine subsets were used in calculating S_y. This provided $N=34$ points. The value of k was determined by the total number of constants fitted in Eq. 13. The centroid $(\bar{X}_j, \bar{Y}_j)$ of each of the nine data subsets was fitted. There were no fitted constants in the classical strength theories, however, two constants (a and b) were previously fitted for the new strength model. Since these

TABLE 3 SUMMARY OF STATISTICAL RESULTS PARTITIONING RUPTURE-TIME ERROR AT EACH STRESS STATE INTO STRENGTH THEORY AND RANDOM SCATTER (MATERIAL AND TESTING) ERROR COMPONENTS

$R=\frac{\sigma_\theta}{\sigma_z}$	BIAXIAL ANGLE $\theta°$	STATISTICAL ANALYSIS RESULTS FOR STRENGTH THEORY SHOWN *							
		NEW		VON MISES		TRESCA		RANKINE	
		10^{a}	10^{a+2S_y}	10^{a}	10^{a+2S_y}	10^{a}	10^{a+2S_y}	10^{a}	10^{a+2S_y}
0.00	0.0	1.56	2.90	1.56	2.90	1.56	2.90	1.56	2.90
0.17	9.7	1.29	2.40	1.11	2.07	1.56	2.90	1.48	2.76
0.25	14.0	1.60	2.97	1.30	2.41	2.06	3.84	1.91	3.56
0.50	26.6	1.17	2.19	0.85	0.45	1.57	2.92	1.35	2.51
0.67	33.8	1.96	3.66	1.36	2.53	2.30	4.28	1.89	3.51
0.75	36.9	0.88	0.48	0.61	0.33	0.93	0.50	0.74	0.40
1.00	45.0	1.44	2.69	0.99	0.53	0.99	0.53	0.73	0.39
1.20	50.2	1.15	2.14	0.79	0.43	1.07	1.99	0.80	0.43
1.33	53.1	0.79	0.42	0.55	0.30	0.84	0.45	0.62	0.34
1.50	56.3	0.86	0.46	0.61	0.33	1.02	1.90	0.76	0.41
1.60	58.0	0.75	0.40	0.53	0.29	0.93	0.50	0.69	0.37
1.71	59.7	0.77	0.41	0.56	0.30	1.00	1.86	0.75	0.40
1.85	61.6	0.63	0.34	0.46	0.25	0.85	0.46	0.63	0.34
2.00	63.4	0.51	0.28	0.38	0.21	0.71	0.38	0.53	0.28
4.00	76.0	0.62	0.33	0.53	0.29	0.86	0.46	0.66	0.35
∞	90.0	0.60	0.32	0.65	0.35	0.74	0.40	0.55	0.30
-0.25	104.0	0.95	0.51	6.09	11.33	9.05	16.84	3.46	6.45
-1.00	135.0	1.04	1.94	3.19	5.95	5.91	11.00	0.30	0.16
-2.00	153.4	0.83	0.45	1.61	2.99	2.63	4.89	0.46	0.25
-4.00	166.0	0.80	0.43	1.16	2.16	1.54	2.86	0.59	0.32

* Numbers >1.0 indicate life underprediction (conservative)
<1.00 indicates life overprediction (non-conservative)

S_y= statistical standard error computed from the random errors, ϵ_{ij}, for the total biaxial data set in Table 1

= 0.1349 (10^{2S_y} =1.86)

$$10^{a} = \left[\frac{\text{average observed biaxial life at the designated stress state}}{\text{predicted life based on the uniaxial correlation, Eq. 8, and equivalent stress, } \sigma_e\text{, for the designated strength theory}}\right]$$

$$10^{a+2S_y} = \left[\frac{\text{average observed biaxial life at the designated stress state + 2 standard errors}}{\text{predicted life based on the uniaxial correlation, Eq. 8, and equivalent stress, } \sigma_e\text{, for the designated strength theory}}\right]$$

two constants are associated with stress state (i.e., with α_j) and not with material and testing variability (i.e. not with ϵ_{ij}) they were not included in Eq. 14. The value of k used was, therefore, 9 for all the strength theories. For those stress states in Table 1 having only one data point, this point was taken as the centroid $(\bar{X}_j, \bar{Y}_j)$ for that stress state (i.e., stress state effect). No attempt was made to statistically quantify the uncertainty associated with the α_j values since these values do not satisfy the conditions for a Gaussian distribution.

Results of the statistical analysis are summarized in Table 3. Although the error components were determined in linear log (stress) vs log (rupture time) space, the antilogs of the resulting α_j and S_y values are summarized in Table 3 and represent factors on life. Analysis results indicate that the random error (i.e., $\pm 2S_y$ which was attributed to material and testing variablility) introduced a factor of ~ 1.86 (as a multiplier or as a divider) on life. Factors on life due to strength-theory error (antilog of α_j) are stress-state dependent as was obvious from Figs. 5-8. The further the factors summarized in Table 3 deviate from 1.0, the greater the strength-theory error. For stress states in the tension-compression quadrant these factors were significantly greater than the factors associated with material and testing variability. Considering the results in Table 3 as a whole (i.e., divide the most conservative factor by the most nonconservative factor for each theory), then the new strength theory provided the least range of error (13.1) followed by the Rankine (40.3), Tresca (44.3), and von Mises (53.9) theories in that order.

CONCLUSIONS

The new multiaxial stress-rupture strength theory resulted in significantly improved life predictions for specimens of annealed Inconel 600 tested at 816°C in argon under different biaxial stress states. The improvement for Inconel was not as great and as dramatic as reported earlier for Types 304 and 316 stainless steel, however the improvement was still quite significant. The scatter in stress vs rupture time data was reduced by a factor of about 2.4 (on life) relative to scatter for the theories of Mises and Tresca and by a factor of about 5 relative to the Rankine theory. As was found in the earlier papers on 304 and 316 stainless steel, theory errors, α_j, for the new theory tended to be about the same magnitude for the various biaxial stress states evaluated whereas errors for the classical theories tended to be significantly larger in the T-C quadrant of stress space than in the T-T quadrant.

REFERENCES

1. R. L. Huddleston, "An Improved Multiaxial Creep-Rupture Strength Criterion," *Trans. ASME*, Vol. 107, No. 4, pp. 313-438 (1984).

2. R. L. Huddleston, "Assessment of An Improved Multiaxial Strength Theory Based on Creep-Rupture Data for Type 316 Stainless Steel," pp. 23-31 in *Stress Classification, Robust Methods, and Elevated Temperature Design, proceedings of the 1992 Pressure Vessel and Piping Conference, New Orleans, La., June 21-25, 1992*, ed. C. Becht IV, R. Seshadri, and D. Marriott, American Society of Mechanical Engineers, New York, 1992.

3. S. Timoshenko, *Strength of Materials*, Third ed., D. Van Nostrand Company, Inc., New York, 1956, pp. 444-462.

4. Code Case N47-29, Class I Components in Elevated Temperature Service, Section III, Division 1, *Cases of ASME Boiler and Pressure Vessel Code*, American Society of Mechanical Engineers, New York, 1990.

5. Chubb, E. J., and Bolton, C. J., "Stress State Dependence of Creep Deformation and Fracture in AISI Type 316 Stainless Steel," pp. 39-48 in *International Conference on Engineering*

Aspects of Creep, September 15-19, 1980, Vol. 1, Mech. Eng. Publ. Ltd. for Inst. of Mech. Engineers, London, 1980.

6. Kennedy, C. R., Harms, W. O., and Douglas, D. A., "Multiaxial Creep Studies on Inconel at 1500°F," *Trans. ASME*, Vol. 81, pp. 599-609 (1959).

7. Rabotnov, Y. N., *Creep Problems in Structural Members*, tr. Transcripia Service Ltd., London, tr. ed., F. A. Leckie, North-Holland Publishing Co., Amsterdam, 1969, pp. 393-396.

8. Davis, E. A., "Creep Rupture Tests for Design of High-Pressure Steam Equipment," *Trans. ASME*, Vol. 82, pp. 453-461 (1960).

9. Johnson, A. E., Henderson, J., and Khan, B., *Complex-Stress Creep, Relaxation, and Fracture of Metallic Alloys*, National Engineering Laboratory, East Kilbride, Glasgow, Scotland, Feb. 1962.

10. Rowe, G. H., Stewart, J. R., and Burgess, K. N., "Capped End, Thin-Wall Tube Creep-Rupture Behavior for Type 316 Stainless Steel," *ASME Journal of Basic Engineering*, Vol. 85, pp. 71-86 (Mar. 1963).

11. Abo El Ata, M. M., and Finnie, I., "On the Prediction of Creep-Rupture Life of Components Under Multiaxial Stress," pp. 80-95 in *International Union of Theoretical and Applied Mechanics, Second Symposium on Creep in Stuctures, Gothenburg, 1970*, Springer-Verlag, Berlin, 1972.

12. Hayhurst, D. R., "Creep Rupture Under Multiaxial States of Stress." *Journal of Mech. Phys. Solids*, Vol. 20, pp. 381-390 (1972).

13. Anderson, W. J., Atkins, D. F., and Shively, J. H., *Mechanical Properties of Stainless Steels in Sodium, and Application to LMFBR Design*, A1-AEC-1300, Atomics International, Feb. 1972.

14. Hayhurst, D. R., Leckie, F. A., and Morrison, C. J., *A Continuum Damage Study of Notched Strengthening and Weakening in Creep Rupture*, Report 77-3, Engineering Department, University of Leicester, Leicester, England, Jan. 1977.

15. Manjoine, M. J., "Multiaxial Stress and Fracture," *Fracture*, Vol. 3, pp. 265-309 (1971).

16. Cane, B. J., "Creep Damage Accumulation and Fracture Under Multiaxial Stresses," pp. 1285-1293 in *Advances in Fracture Research, Fifth International Conference on Fracture*, Vol. 4, Pergamon Press, Oxford, 1981.

17. Speight, M. V., and Beere, W., "Vacancy Potential and Void Growth on Grain Boundaries," *Metals Science Journal*, Vol. 9, p. 198 (1975).

18. Beere, W., and Speight, M. V., "Creep Cavitation by Vacancy Diffusion in Plastically Deforming Solids," *Metals Science Journal*, Vol. 12, pp. 172-176 (April 1978).

19. Hellan, K., "An Approximate Study of Void Expansion by Ductility or Creep," *International Journal of Mechanical Science*, Vol. 17, p. 369 (1975).

20. Dyson, B. F., "Constraints on Diffusional Cavity Growth Rates," *Metals Science Journal*, Vol. 10, pp. 349-353 (1976).

DISCLAIMER

DATE
FILMED
9/9/93

END